Structures, Structural Dynamics, and Materials and Co-located Conferences
April 8-11, 2013, Boston, Massachusetts
54th AIAA/ASME/ASCE/AHS/ASC Structures, Structural Dynamics, and Materials Conference

SDM 2013 Student Papers Competition
Modeling fiber-matrix splitting failure through a mesh-objective continuum-decohesive finite element method

Pavana Prabhakar*and Anthony M Waas†

A new finite element formulation that can seamlessly model the transition from a continuum to a non-continuum (through fracture) is introduced in this paper. In-plane fiber-matrix fracture (also referred to as splitting) is frequently observed in tensile failure of fiber reinforced polymer matrix composites (FRPC). This mechanism is modeled through the development of a continuum-decohesive finite element (CDFE) by considering a single lamina. The transition from a continuum to a non-continuum in the CDFE method is modeled directly (physically) without resorting to enrichment of the shape functions of the element, as is done in other methods, such as the variational multiscale cohesive method (VMCM) or through nodal enrichment as in extended finite element method (XFEM). The CDFE is a natural merger between cohesive elements and continuum elements. Predictions using the CDFE method were found to be in very good agreement with corresponding experimental data for open hole tension tests of fiber reinforced lamina.

I. Introduction

A new finite element to model fiber-matrix in-plane fracture of fiber reinforced laminated composites is formulated. The formulation is motivated by the variational multiscale cohesive method (VMCM) as described in,[1] where the displacement field is additively decomposed into a coarse and fine scale. Subsequently, by using the principle of virtual work (PVW), the governing equations for the two scales are obtained. In VMCM, both the fine scale and coarse scale are captured through the incorporation of new shape functions that facilitate the capturing of sharp gradients across discontinuities. In the CDFE formulation, the discontinuity is modeled as a physical separation (fracture) within an element, as opposed to a two-scale enrichment of the shape functions. The two sub-elements of a fractured element are connected through a traction-law that embeds the fracture properties of the discontinuity, and its evolution. The two sub-elements are modeled as standard continuum elements, however the discontinuity is captured through an assumed traction-law. Thus, the CDFE is seen as a natural merger between continuum elements and the discrete cohesive zone elements (DCZM),.[2]

This paper is organized as follows; Section III provides the mathematical formulation for the CDFE, along with a discussion regarding the input material properties required; continuum to non-continuum transition criteria are discussed in Section IV; the details of the finite element implementation are given in Section V, followed by examples of open hole tension predictions of 90, 45 and 0 degree lamina.

It is well known that the regular finite element formulation can be used as long as the material constitutive law has a positive tangent modulus throughout the loading considered,.[3] But, when fracture emerges, the local tangent modulus ceases to be positive definite. Incorporating constitutive laws that display a negative tangent stiffness in a regular finite element setting leads to pathologically mesh dependent solutions. That is, the solution to the boundary value problem becomes ill-posed, with the solution being dependent on element size. Several remedies to this situation have been discussed, and successfully implemented as demonstrated in, for example,.[3]

*Graduate Student, Department of Aerospace Engineering, 1320 Beal Avenue, Ann Arbor, MI 48109-2140. AIAA Student Member.

†Felix Pawlowski Professor of Aerospace Engineering, Department of Aerospace Engineering, 1320 Beal Avenue, Ann Arbor, MI 48109-2140. Fellow, AIAA.

II. Summary of Related Prior Work

Several methods have been formulated to model two-piece failure (characterized through a material constitutive law consisting of a softening region) as shown in Fig. 1. If the crack path in a model is known a-priori, discrete cohesive zone method (DCZM) elements can be placed between potential surfaces along the crack path (,[24]). These elements follow a traction-separation law between them, where the traction on the new surfaces is a function of the separation between the surfaces. The DCZM elements have a very high initial stiffness, which results in almost perfect adhesion between the surfaces. Then, as the element reaches the cohesive strength of the material, the element begins to unload following the traction-separation law.

A smeared crack band approach was developed by,[5] which introduced a characteristic element length into the post-peak softening damage evolution formulation. The softening part of the stress-strain relation was scaled by a characteristic length of the material to ensure that the total energy released due to failure is equal to the fracture toughness of the material, regardless of the element size. Further developments of this approach to account for mixed-mode failure was carried out by,[6],[7],[8][9] and.[10]

Other methods available fall under the category of enrichment methods, where the shape functions are modified to account for discontinuities within the elements. Nodal enrichment methods, such as the extended FEM (XFEM) presented in,[11],[12] and element enrichment methods, such as the variational multiscale cohesive method (VMCM) presented in,[13][14] and,[1] model discontinuities in a continuum by embedding fine scale fields into a coarse scale field in the finite element formulation. The fine scale fields evolve following a cohesive law in the form of a traction - separation law, resulting in mesh objectivity. Since, the elements are embedded with a discontinuity (or multiple discontinuities) within them, the crack path(s) evolution need not be known a-priori. A comparison of enrichment methods is reported in.[15]

The current CDFE method is motivated by the VMCM Method, where the crack path traverses through the element, in the form of discontinuity. The basic difference between the VMCM and the CDFE is that the discontinuity is modeled physically in an element in CDFE, as opposed to shape function enhancement as in the case of VMCM. The regular shape functions in VMCM are enhanced with a discontinuous shape function to account for the discontinuity in the medium. The discontinuity in CDFE is inserted by fracturing the element into two parts, and the newly created interface tractions are governed by a cohesive traction-separation law. Therefore, the CDFE method results in a straight-forward formulation and implementation as compared to the VMCM. It also finds ready insertion into available FE codes, since standard shape functions are used throughput.

III. Mathematical formulation - Principle of Virtual Work (PVW)

In the CDFE formulation, a fractured body (non-continuum) is treated differently from a continuum that has no crack. That is, the PVW for a continuum body, occupying the domain Ω, and limited to the infinitesimal theory of elasticity (refer to Fig. 2(a)), is given by,

$$\int_{\Omega} \nabla w : \sigma dV = \int_{\Omega} w f dV + \int_{\Gamma_h} w T dS \tag{1}$$

where Γ_h is the traction boundary, w is the virtual displacement field, f is the body force field, T is the prescribed external traction, σ is the Cauchy stress tensor ($\sigma = D : sym(\nabla u)$), where D is the elasticity tensor, and u is the displacement field of the domain.

Next, consider the same body, but containing, within its domain, a surface across which the displacement field is discontinuous. Applying the PVW for a cracked body (refer to Fig. 2(b)) results in,

$$\begin{aligned} \int_{\Omega_1} \nabla w : \sigma \, dV + \int_{\Omega_2} \nabla w : \sigma \, dV - \int_{\Gamma_3} w \, T([[u]]) dS = \\ \int_{\Omega_1} w \, f \, dV + \int_{\Gamma_{h_1}} w \, T \, dS + \int_{\Omega_2} w \, f \, dV + \int_{\Gamma_{h_2}} w \, T \, dS \end{aligned} \tag{2}$$

where, the interface Γ_3 separates the domain Ω into two domains, Ω_1 and Ω_2. The traction across the two new surfaces of the two separated domains is related to the jump displacements (the displacement discontinuity) through a traction-separation law. That is, the traction is a function of the jump displacements given by $T([[u]])$, where $[[u]]$ denotes the displacement jump. The tractions do work over the jump displacements as the

body separates into two pieces. Fig. 2(c) and Fig. 2(d) show traction laws, where the jump displacement can reverse sign. A 2-D cohesive traction separation law is used that defines the fracture process in departure from a continuum. Two traction-separation laws are used; one each for mode-I (opening) and mode-II (sliding). The mode-I cohesive law, which signifies displacement jumps perpendicular to the fracture surface, in the local coordinate system is,

$$\begin{aligned} T_1 &= \sigma_{IC}\left[1-\frac{\delta_I}{\delta_{Im}}\right] \quad \text{if} \quad \delta_I > 0, \Delta\delta_I >= 0 \\ T_1 &= \bar{k}_I \delta_I \quad \text{if} \quad \delta_I > 0, \Delta\delta_I < 0 \quad \text{where,} \quad \bar{k}_I = \frac{\sigma_I^\star}{\delta_I^\star} \end{aligned} \tag{3}$$

Similarly, the mode-II cohesive law, which signifies tangential displacement jumps, in the local coordinate system is given by,

$$\begin{aligned} T_2 &= \sigma_{IIC}\left[1-\frac{\delta_{II}}{\delta_{IIm}}\right] \quad \text{if} \quad \delta_{II} > 0, \Delta\delta_{II} >= 0 \\ T_2 &= \bar{k}_{II} \delta_{II} \quad \text{if} \quad \delta_{II} > 0, \Delta\delta_{II} < 0 \quad \text{where,} \quad \bar{k}_{II} = \frac{\sigma_{II}^\star}{\delta_{II}^\star} \\ T_2 &= -\sigma_{IIC}\left[1-\frac{|\delta_{II}|}{\delta_{IIm}}\right] \quad \text{if} \quad \delta_{II} <= 0, \Delta\delta_{II} < 0 \\ T_2 &= \bar{k}_{II} \delta_{II} \quad \text{if} \quad \delta_{II} <= 0, \Delta\delta_{II} > 0 \quad \text{where,} \quad \bar{k}_{II} = \frac{-\sigma_{II}^\star}{-\delta_{II}^\star} \end{aligned} \tag{4}$$

where, δ_I and δ_{II} are the jump displacements in mode-I and mode-II between the decohered surfaces of the fractured continuum, and $\Delta\delta_I$ and $\Delta\delta_{II}$ are the corresponding change in the jump displacements between load increments in FEM. Though a triangular traction - separation law is used here, it should be noted that no restrictions on the nature of the traction law are imposed in CDFE.

It is noted that, just as in the VMCM and unlike in other cohesive zone implementations, the emergence of the traction - separation law is at a finite value of the traction. In classical cohesive zone implementations, the traction - separation law emerges from the origin, since such elements are used from the inception of loading, whereas, the emergence of fracture at a finite traction, which is physically correct, is captured in the VMCM and CDFE. Other cohesive zone models thus require a "penalty stiffness", which defines the initial portion of the traction - separation law. This aspect has also been pointed out in earlier work by.[16] Thus, in the CDFE, the *process* of fracture is captured through the traction-jump displacement law. In classical fracture mechanics, the *process* of fracture is not captured in a continuous manner, instead two fractured states, which correspond to two different crack lengths, are treated as isolated states of equilibrium.

Using Equation 1 for the intact continuum, and Equation 2 for a fractured continuum, the corresponding finite element equations are derived in the following sections.

The material properties required for the CDFE method are discussed below. Since, fiber reinforced lamina is the focus, a transversely isotropic material system is considered. The corresponding transversely isotropic linear elastic material inputs are E_1, E_2, ν_{12} and G_{12} in a plane stress setting. The fiber orientation angle in a lamina is θ, which imparts directionality to the lamina. The cohesive input properties are the in-plane fracture toughnesses and the cohesive strengths (G_{IC}, G_{IIC}, σ_{IC}, σ_{IIC}).

IV. Transition from a Continuum to a Non-Continuum

The transition criterion required to signal the emergence of a displacement jump is discussed next. A stress based criterion is adopted here. The evolution of the failure/fracture of the continuum is based on a mixed mode energy release criterion. In fiber reinforced lamina, the failure orientation is influenced significantly by the presence of fibers. That is, since the fibers have strengths that are two orders of magnitude larger compared to the matrix material, the failure direction is dominated by the direction of the fiber. In the present study, both fracture perpendicular and parallel to the fibers, are considered.

For fracture perpendicular to the fiber direction (θ), as shown in Fig. 3(a), the fracture initiation condition

is,

$$\left(\frac{\sigma_{11}}{\sigma_C^f}\right) \geq 1 \tag{5}$$

where, σ_{11} is the tensile stress along the fiber direction, and σ_C^f is the cohesive strength of the fiber.

For fracture parallel to the fiber direction (θ), as shown in Fig. 3(b) and Fig. 3(c), the following transition condition is used,

$$\left(\frac{\sigma_{22}}{\sigma_C^m}\right)^2 + \left(\frac{\sigma_{12}}{\tau_C^m}\right)^2 \geq 1 \tag{6}$$

where, σ_{22} and σ_{12} are the transverse and shear stresses in the rotated coordinate system, and 1 is along the fiber direction. σ_C^m and τ_C^m are the cohesive strengths in mode-I and mode-II in the matrix. Since the cohesive strength of the fibers is usually very high compared to that of the matrix material, the matrix failure occurs prior to fiber failure in a lamina, usually in the presence of multi-axial loading.

In the non-continuum state, fracture evolution is assumed to be governed by a mixed mode energy release criterion given by:

$$\frac{G_I}{G_{IC}} + \frac{G_{II}}{G_{IIC}} \geq 1 \tag{7}$$

where, δ_I is separation perpendicular to the fracture path (Mode-I or opening mode), δ_{II} is the separation along the fracture path (Mode-II or sliding mode), G_I is the fracture energy dissipated corresponding to δ_I from Mode-I cohesive law, G_{II} is the fracture energy dissipated corresponding to δ_{II} from Mode-II cohesive law, G_{IC} is the fracture toughness of Mode-I cohesive law and G_{IIC} is the fracture toughness of Mode-II cohesive law. The above criterion is widely used for fiber reinforced composites, and has been demonstrated in papers.[17–21]

V. Finite Element Formulation

The equations resulting from the application of the PVW to a continuum and a fracturing continuum are discretized to obtain the corresponding finite element equations. In the continuum (Ω), the domain is divided into a finite number of elements. The presentation of the formulation is restricted to two dimensional triangular elements, for illustrative purpose, whose nodal displacements are given by, $U^e = [u_1\ u_2\ u_3\ u_4\ u_5\ u_6]^T$ (refer to Fig. 4(a)). It is noted that the method introduced here is independent of the choice of element type.

The displacement field $\{u^e\}$ and the virtual displacement field $\{w^e\}$ of each element, in terms of nodal displacements are given by, $\{u^e\} = [N]_{(1,6)}\ \{U^e\}_{(6,1)}$ and $\{w^e\} = [N]_{(1,6)}\ \{W^e\}_{(6,1)}$.

Substituting the above equations into Equation 1, the residual ($\{r\}$) of the finite element equations for an uncracked body (Ω) is derived as,

$$\{r\} = \int_\Omega B^T\ D : Bu\ dV - \int_\Omega N f\ dV - \int_{\Gamma_h} N\ T\ dS \tag{8}$$

where B is the strain-displacement relation. After linearizing, the above equations are solved to determine the nodal displacements. The corresponding stresses in each element are determined, and checked for transition.

When a transition criterion is met in an element, the element fractures in accordance with the specified traction laws, as shown in Fig. 4(b). The black nodes in Fig. 4(b) are the original nodes of the element, and the white nodes are two new nodes that emerge due to element fracture. The crack path is parallel or perpendicular to the fiber direction and cuts across the integration point of the continuum element. To develop the reduced stiffness matrix, consider the additional (dummy) nodes along the fracture path. The interface tractions follow a cohesive traction-separation law as shown in Fig. 2(c) or Fig. 2(d). Equation 2 can be rearranged as follows:

$$\begin{aligned}\int_{\Omega_1} \nabla w : \sigma\ dV + \int_{\Omega_2} \nabla w : \sigma\ dV + \int_{\Gamma_3} w\ T_1(\delta_I) dS + \int_{\Gamma_3} w\ T_2(\delta_{II}) dS = \\ \int_{\Omega_1} w\ f\ dV + \int_{\Gamma_{h_1}} w\ T\ dS + \int_{\Omega_2} w\ f\ dV + \int_{\Gamma_{h_2}} w\ T\ dS\end{aligned} \tag{9}$$

where, δ_I and δ_{II} are the mode-I and mode-II jump displacements of the interface in a cracked element. Also, $\{\sigma\} = [D]\{\epsilon\}$, where $[D]$ is the constitutive material matrix of the individual sub-elements, $\{\epsilon\}$ is strain vector ($\{\epsilon\}$=f($\frac{\delta u_i}{\delta x_i}$), i=1,2) in each of the two domains Ω_1 and Ω_2.

The enhanced residual can then be expressed as,

$$\begin{aligned}\{R\} = \int_{\Omega_1} \nabla w : \sigma \; dV + \int_{\Omega_2} \nabla w : \sigma \; dV - \int_{\Gamma_3} w \; T_1(\delta_I) dS - \int_{\Gamma_3} w \; T_2(\delta_{II}) dS \\ - \int_{\Omega_1} w \; f \; dV - \int_{\Gamma_{h_1}} w \; T \; dS - \int_{\Omega_2} w \; f \; dV - \int_{\Gamma_{h_2}} w \; T \; dS\end{aligned} \tag{10}$$

In the cracked, but not completely decohered element, sub-element 1 has local nodal displacements given by, $\{u\} = [u_1 \; u_2 \; u_3 \; u_4 \; u_7 \; u_8 \; u_9 \; u_{10}]^T$ and sub-element 2 has local nodal displacements given by, $\{u\} = [u_{11} \; u_{12} \; u_{13} \; u_{14} \; u_5 \; u_6]^T$ as shown in Fig. 4(c). The corresponding virtual nodal displacements are $\{w^e\} = [w_1 \; w_2 \; w_3 \; w_4 \; w_7 \; w_8 \; w_9 \; w_{10}]^T$ and $\{w\} = [w_{11} \; w_{12} \; w_{13} \; w_{14} \; w_5 \; w_6]^T$. The terms of Equation 9 can be expressed in terms of the following displacement fields:

$$\begin{aligned}\int_{\Omega_1} \nabla w : \sigma \; dV &= \{w_1\}^T_{(6,1)} \left[\int_{\Omega_1} \mathbf{B_1^T D B_1} \; dV\right]_{(6,6)} \{U_1\}_{(6,1)} \\ \int_{\Omega_2} \nabla w : \sigma \; dV &= \{w_2\}^T_{(8,1)} \left[\int_{\Omega_2} \mathbf{B_2^T D B_2} \; dV\right]_{(8,8)} \{U_2\}_{(8,1)} \\ \int_{\Gamma_{h_1}} w \; T \; dS + \int_{\Omega_1} w \; f \; dV &= \{w_1\}^T_{(6,1)} [F_1]_{(6,1)} \\ \int_{\Gamma_{h_2}} w \; T \; dS + \int_{\Omega_2} w \; f \; dV &= \{w_2\}^T_{(8,1)} [F_2]_{(8,1)} \\ \int_{\Gamma_3} w \; T_1(\delta_I) dS + \int_{\Gamma_3} w \; T_2(\delta_{II}) dS &= \{w_3\}^T_{(8,1)} \; T(\delta_I, \delta_{II})\end{aligned} \tag{11}$$

where, B_1 and B_2 are strain-displacement relations of Ω_1 and Ω_2. δ_I and δ_{II} are mode-I and mode-II jump displacements at the interface between Ω_1 and Ω_2.

Linearizing Equation 10 and rearranging the terms, we obtain an enhanced system of equations corresponding to enhanced nodal displacement field given by, $U_e = [u_e \; \hat{u}_e]^T$, where, $u_e = [u_1 \; u_2 \; u_3 \; u_4 \; u_5 \; u_6]^T$, and $\hat{u}_e = [u_7 \; u_8 \; u_9 \; u_{10} \; u_{11} \; u_{12} \; u_{13} \; u_{14}]^T$.

The corresponding enhanced element stiffness matrix and force vector are given by,

$$K_e = \begin{bmatrix} K^e_{11(6,6)} & K^e_{12(6,8)} \\ K^e_{21(8,6)} & K^e_{22(8,8)} \end{bmatrix} \qquad F_e = \begin{bmatrix} F_{e(6,1)} \\ \hat{F}_{e(8,1)} \end{bmatrix}$$

¿From static condensation, the equivalent stiffness matrix and the force vector of the element can be derived as,

$$[K^e_{11} - K^e_{12} {K^e_{22}}^{-1} K^e_{21}]\{u_e\} = \{\bar{F}_e\} \quad , \quad \{\bar{F}_e\} = \{F_e\} - K^e_{12} {K^e_{22}}^{-1} \{\hat{F}\}$$

Therefore, the equivalent stiffness of the cracked element is,

$$[K^{eq}_e] = [K^e_{11} - K^e_{12} {K^e_{22}}^{-1} K^e_{21}] \quad , \quad [K^{eq}_e]\{u_e\} = \{\bar{F}_e\}$$

Thus, the contribution of the decohered element to the global system is through the original nodal displacements of the continuum triangle element. $[K_e]$ has contributions from the two sub-elements (triangular element and quadrilateral element) and the interface tractions. The stiffness contributions of the triangular and quadrilateral elements are derived in the same way as any regular continuum element. The entire procedure for implementing the CDFE method is illustrated in Fig. 5.

VI. Open Hole Tension Simulations : Fracture of Matrix Parallel to Fiber Direction

The above finite element formulation has been implemented in an in-house code through a high-level technical computing language and interactive environment within MATLAB. The method is demonstrated by modeling the open hole tension test of 90, 45 and 0 degree lamina, for which a set of experimental results is also available. The lamina material properties were measured through in-house experiments on a proprietary material similar to IM7/8552, and are as follows: E_{11}=136 GPa, E_{22}=6.7 GPa, ν_{12}=0.33, G_{12}=3.2 GPa; In addition, the mode I and mode II fracture toughness values are, 0.67 N/mm and 1.67 N/mm respectively, and the mode I and mode II cohesive strengths are 60 MPa and 90 MPa, respectively.

Fig. 6(a) shows the schematic of an open hole specimen subjected to tension. The fiber orientation angle θ is 90 degrees. The corresponding load-load-point extension plots, which show the unstable failure paths for different mesh sizes, are given in Fig. 6(b).

Mesh refinement is carried out along the expected crack path to investigate the influence of mesh size on the global response of the model, as well as to establish that there is no pathological mesh dependency, as shown in Fig. 7(a) and Fig. 7(b). Similar mesh refinement is also carried out for the 45 degree and 0 degree lamina tensile tests investigated further.

Figures 7(c), 7(d) and 7(e) show the evolving displacements and subsequent cracking of a transversely loaded single ply. Fine mesh shown in Fig. 7(b) was used in this simulation. At a critical value of the far-field tension, fracture in mode-I (opening mode), with a crack propagating along the fiber direction (parallel to the fibers) is seen to emerge at the edge of the hole and propagates uninhibitedly, rendering catastrophic failure.

Similarly, the tensile response of an open hole lamina with fiber orientation $\theta = 45$ degrees (shown in Fig. 8(a)) with respect to the loading direction is also demonstrated. The load - load point displacement responses are plotted for different mesh densities and compared with experimental results in Fig. 8(c). It should be noted here that, the simulation with 1114 elements does not have enough elements for the FEM stress solution to converge, and therefore, it does not fall in the pathological mesh dependency case study.

Here, mixed mode fracture is observed. That is because, along the crack path, both the shear tractions and normal tractions are found to be active. Since the crack is constrained to grow along the fibers or perpendicular to the fibers, the crack tip stress state will involve a combination of stresses. It is observed that the lamina fractures at an angle 45 degrees to the loading direction, as shown in Fig. 9.

Tensile tests were conducted on open hole specimens with fibers orientated at 45 degrees to the loading direction. The face of the laminate was speckled with black dots on a white surface. Images were recorded at fixed intervals during testing. The speckle data was analyzed using digital image correlation (DIC) method to obtain the strain fields. The axial strain field, i.e. along the x-direction, is shown in Fig. 10(a) and Fig. 10(b) at an initial loading stage and at the peak load, respectively. The predicted strain behavior of the 45 degree lamina, shown in Fig. 10(c) and Fig. 10(d), corresponding to an initial loading stage and at the peak load, matches well with the experiments.

Finally, a 0 degree lamina with a hole subjected to tension is studied. A schematic of the model is shown in Fig. 11(a). The load - load point displacement responses are plotted for different mesh densities and compared with experimental results in Fig. 11(c).

In the model, the loading edges are loaded in a displacement controlled manner. It should be noted that the grips are not modeled explicitly in the simulation. Though the cracks start at the hole and propagate towards the loading edges as shown in Fig. 11(b), the two pieces in the model continue to carry load, but with a slightly degraded stiffness. Similar behavior for a notched 0 degree laminate has also been reported in,[22] and simulated using a crack band model in,.[10] The corresponding deformation plots of the lamina are shown in Fig. 12(a), Fig. 12(b) and Fig. 12(c). Whereas, in the experiment, it was observed that as the cracks propagate towards the loading edges, the energy released caused one of the edges to slip out of the grips resulting in the global drop in stress value causing a peak as shown in Fig. 11(c). But, the response appears to change stiffness prior to the global drop in stress. If the specimen had not slipped out of the grips in the test, then the experiment and the simulation response would match completely. Therefore, it can be concluded that the cracks have propagated through the length of the specimen prior to reaching the peak (which is caused due to slipping of grips) in the experimental result (shown in Fig. 11(c)). It can be concluded that the failure of the 0 degree lamina open hole tension test is dominated by mode-II failure, and a characteristic longitudinal crack, which emerges at the hole edge, is seen to propagate away from the hole

and along the fiber direction.

The experimentally obtained strain fields, analyzed through DIC, of a 0 degree lamina was also obtained as in the case of a 45 degree lamina. The splitting fracture occurs along the fiber direction, and propagates through the length of the specimen, starting at the hole edge. Experimental strain fields at an initial stage and at the peak load are shown in Fig. 13(a) and Fig. 13(b), respectively. These shear strain fields obtained from experiment closely match those corresponding to the predictions from numerical simulations (shown in Fig. 13(c) and Fig. 13(d)).

VII. Discussion and Concluding Remarks

The CDFE method can be used to predict in-plane failure by fracture in laminated composites, as demonstrated through the single lamina examples that have been studied. The predictions converge to a single response with mesh refinement. Therefore, pathological mesh dependency is absent in the CDFE method. Fracture by splitting can also be captured by a crack band model,[10] or smeared crack model,,[9] which are weak discontinuity implementations, whereas, the present CDFE method is a strong discontinuity method, allowing the crack path to be independent of the element boundaries, similar to the VMCM method.

As with any post-peak, strain softening capturing numerical method, the predicted response in the post-peak regime is dependent on the characteristic length scales, defined by, $l_1 = \frac{E_{xx}G_{IC}}{\sigma_C^2}$ and $l_2 = \frac{G_{xy}G_{IIC}}{\tau_C^2}$ in mode-I and mode-II, respectively,.[23] That is, stable crack path and response is observed when the lengths l_1 and l_2 are sufficiently large, making the failure more "ductile", whereas, unstable response is observed when these lengths are small compared to the current crack length, rendering the failure to be brittle, as it should. In the case of brittle failure, future work will examine the dynamic equations of motion, since an initiated crack will propagate a finite distance prior to attaining an equilibrium state (if any exists%) For such cases, an explicit solution scheme is more suitable. Notwithstanding these issues, the CDFE can be used for cases that are presently studied using standard cohesive zone methods and VMCM. Furthermore, the CDFE can be implemented in a straight-forward manner, using existing element libraries without recourse to special shape functions for enrichment. Furthermore, extensions to multiple cracking within an element is no more cumbersome than with a single crack, requiring only crack initiation and growth laws, cast in terms of traction-laws.

The open hole lamina tension predictions carried out to demonstrate the CDFE method shows its efficiency in capturing transitions from continuum response to fracture in a seamless manner. The predicted results compared well against experimental results for laminae loaded remotely at different angles to the fiber direction.

VIII. Acknowledgements

The authors are grateful for sponsorship from the Boeing company.

References

[1]Rudraraju, S. S., Salvi, A., Garikipati, K., and Waas, A. M., "In-plane fracture of laminated fiber reinforced composites with varying fracture resistance: experimental observations and numerical crack propagation simulations," *Int J Solids Struct*, Vol. 47(78), 2010, pp. 901–911.

[2]Xie, D. and Waas, "Discrete cohesive zone model for mixed-mode fracture using finite element analysis," *Eng Fract Mech*, Vol. 73, 2006, pp. 1783–1796.

[3]Bazant, Z. and Cedolin, L., *Stability of Structures: Elastic, Inelastic, Fracture, and Damage Theories*, Dover books on engineering, Dover Publ., 1991.

[4]Gustafson, P. and Waas, A., "The influence of adhesive constitutive parameters in cohesive zone finite element models of adhesively bonded joints," *International Journal of Solids and Structures*, Vol. 46, No. 10, 2009, pp. 2201–2215.

[5]Bazant, Z. and Oh, B., "Crack band theory for fracture of concrete," *Materials and Structures*, Vol. 16, 1983, pp. 155–177.

[6]de Borst, R. and Nauta, P., "Non-orthogonal cracks in a smeared finite element model," *Eng. Comput.*, Vol. 2, 1985, pp. 35–46.

[7]Rots, J. and de Borst, R., "Analysis of Mixed-Mode Fracture in Concrete," *J. Eng. Mech.*, Vol. 113(11), 1987, pp. 1739–1758.

[8]Camanho, P., Maim, P., and Dvila, C., "Prediction of size effects in notched laminates using continuum damage mechanics," *Composites Science and Technology*, Vol. 67, No. 13, 2007, pp. 2715–2727.

[9]Heinrich, C. and Waas, A. M., "Investigation of progressive damage and fracture in laminated composites using the

smeared crack approach," *53rd AIAA/ASME/ASCE/AHS/ASC Structures, Structural Dynamics and Materials Conference, 23 - 26 April 2012, Honolulu, Hawaii (AIAA 2012-1537)*, 2012.

[10]Pineda, E. and Waas, A. M., "Modeling progressive failure of fibre reinforced laminated composites: Mesh objective calculations," *Aeronautical Journal*, Vol. 116, 2012, pp. 1221–1245.

[11]Sukumar, N., M. N. M. B. and Belytschko, T., "An extended finite element method (x-fem) for two- and three-dimensional crack modeling," *Numer. Methods Eng.*, Vol. 48(11), 2000, pp. 1741–1760.

[12]Belytschko, T., Mos, N., Usui, S., and Parimi, C., "Arbitrary discontinuities in finite elements," *International Journal for Numerical Methods in Engineering*, Vol. 50, No. 4, 2001, pp. 993–1013.

[13]Garikipati, K. and Hughes, T. J. R., "A study of strain-localization in a multiple scale framework. The one dimensional problem," *Comput Methods Appl Mech Eng*, Vol. 159, 1998, pp. 193–222.

[14]Garikipati, K., "A variational multiscale method to embed micromechanical surface laws in the macromechanical continuum formulation," *CMES-COMPUTER MODELING IN ENGINEERING & SCIENCES*, Vol. 3, No. 2, 2002, pp. 175–184.

[15]Oliver, J., Huespe, A., and Snchez, P., "A comparative study on finite elements for capturing strong discontinuities: E-FEM vs X-FEM," *Computer Methods in Applied Mechanics and Engineering*, Vol. 195, No. 37–40, 2006, pp. 4732–4752.

[16]Jin, Z.-H. and Sun, C. T., "Cohesive Zone Modeling of Interface Fracture in Elastic Bi-Materials," *Engineering Fracture Mechanics*, Vol. 72, 2005, pp. 1805–1817.

[17]Whitcomb, J., "Analysis of instability-related growth of a through-width delamination," *Tech. Rep., NASA*, 1984.

[18]Mi, Y., Crisfield, M., Davies, G., and Hellweg, H., "Progressive delamination using interface elements," *Journal of Composite Materials*, Vol. 32, No. 14, 2012, pp. 1246–1272.

[19]Alfano, G. and Crisfield, M. A., "Finite element interface models for the delamination analysis of laminated composites: mechanical and computational issues," *International Journal for Numerical Methods in Engineering*, Vol. 50, No. 7, 2001, pp. 1701–1736.

[20]Reeder, J., "An evaluation of mixed-mode delamination failure criteria," *Tech. Rep., NASA*, 1992.

[21]Goyal, V. and Klug, J., "Interphasic formulation for the prediction of delamination," *45th AIAA/ASME/ASCE/AHS/ASC Structures, Structural Dynamics and Materials conference, Palm Spring, Ca, April 19-22 (AIAA-2004-1845)*, 2004.

[22]Bogert, P. B., Satyanarayana, A., and Chunchu, P. B., "Comparison of damage path predicions for composite laminates by explicit and standard finite element analysis tool," *47th AIAA Structures, Structural Dynamics, and Materials Conference*, 2006.

[23]Yerramalli, C. S. and Waas, A. M., "A nondimensional number to classify composite compressive failure," *Journal of Applied Mechanics - Transactions of the ASME*, Vol. 71, No. 3, 2004, pp. 402–408.

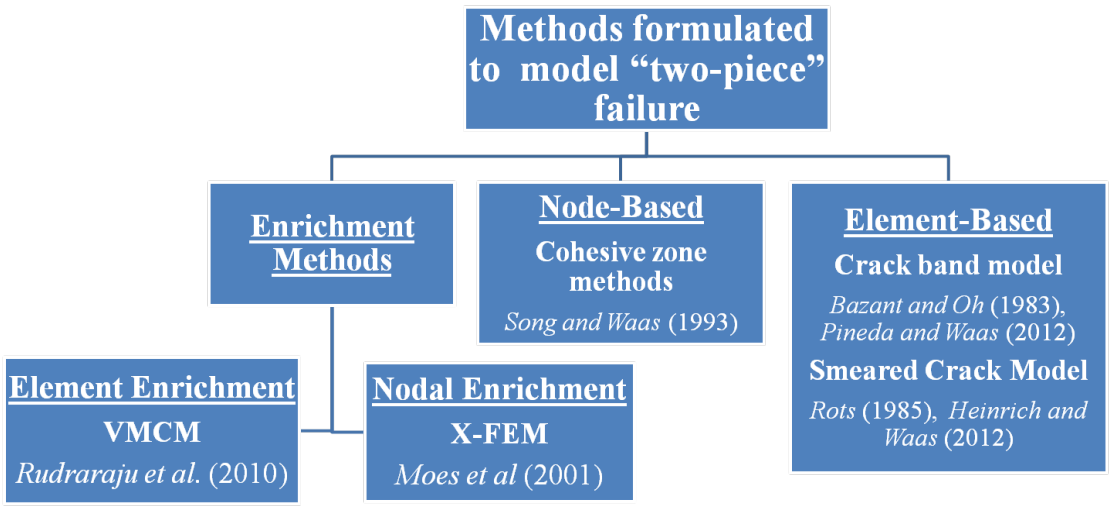

Figure 1. Prior methods formulated to model "two-piece" failure

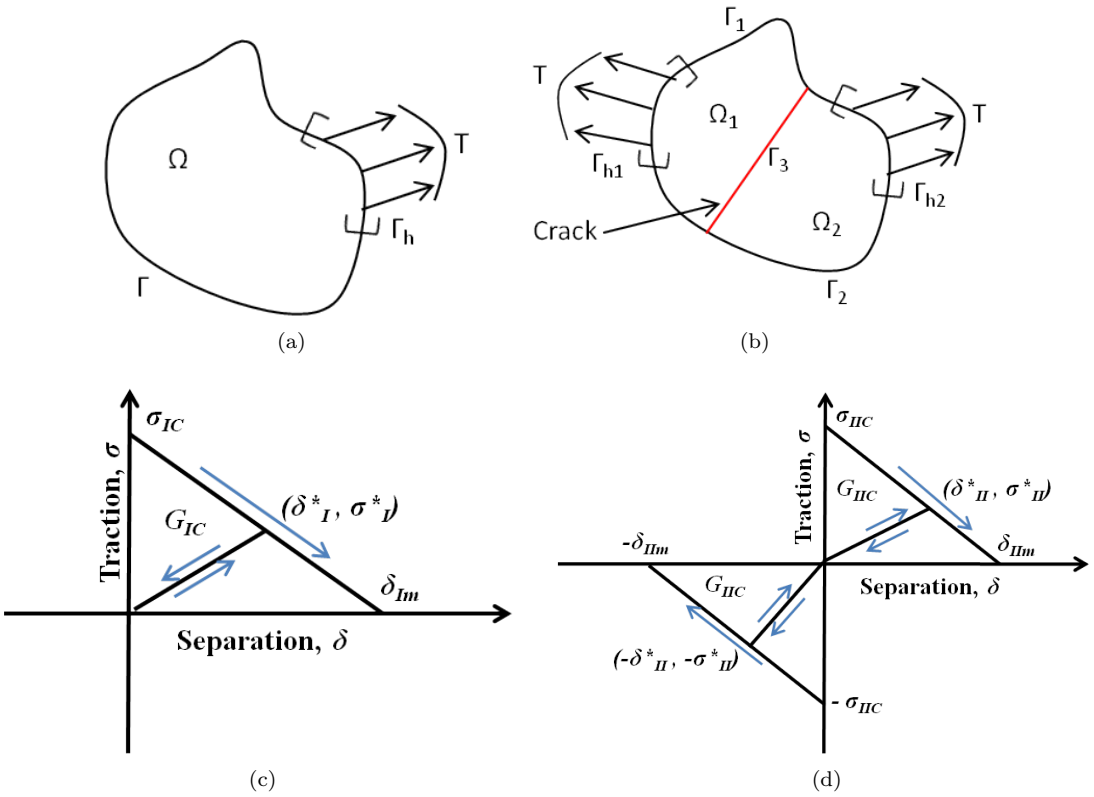

Figure 2. (a) Continuum domain (b) Fractured domain (c) Mode-I cohesive law (d) Mode-II cohesive law

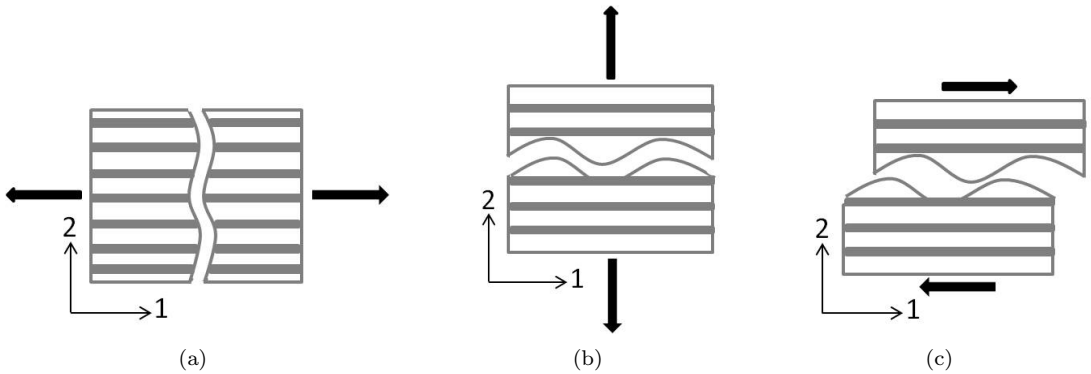

Figure 3. (a) Mode-I fracture perpendicular to the fiber direction (b) Mode-I fracture parallel to the fiber direction (c) Mode-II fracture parallel to the fiber direction

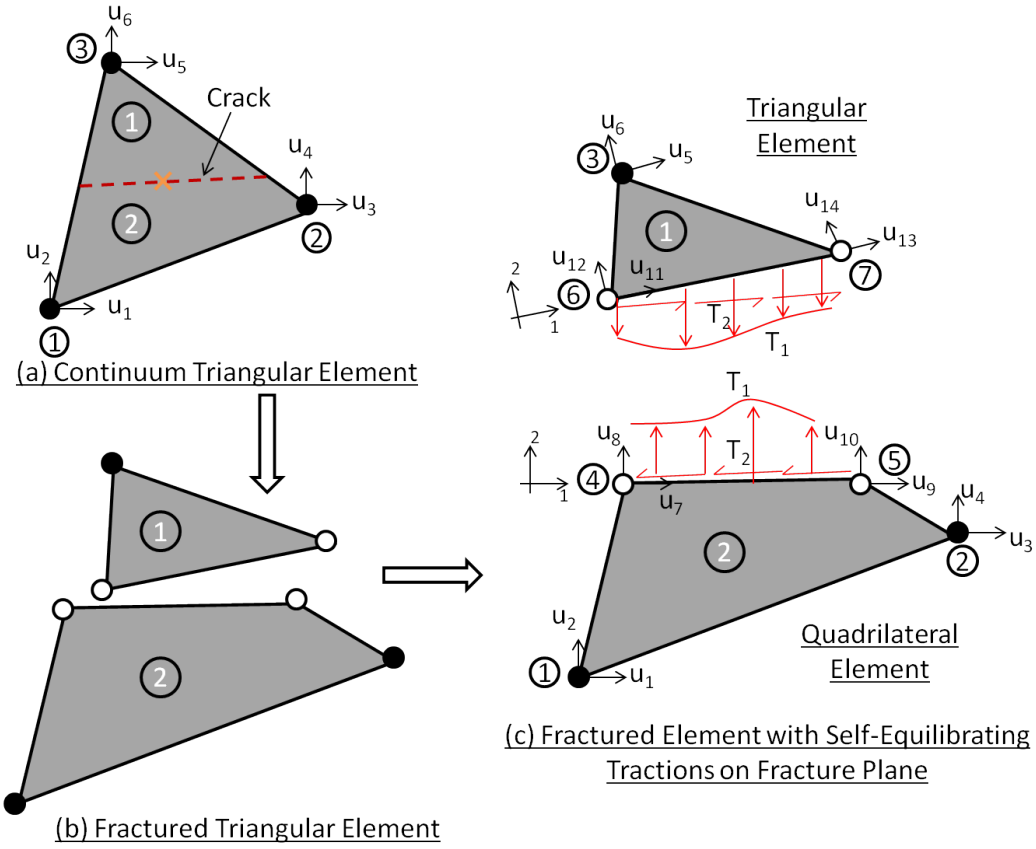

Figure 4. Triangular element: (a) Continuum element, (b) Element with discontinuity (c) Fractured element with discontinuity and interface tractions

1. At increment 'n', $\underline{d}_{n-1}$ is known.
   (a) If 'k' is the current iteration:
   (b) Residual : $\underline{R}\left(\underline{d}^k_{n-1}\right) = \underline{K}\,\underline{d}^k_{n-1} - \underline{f}^{ext}_n$
   (c) If $\underline{R}\left(\underline{d}^k_{n-1}\right) \leq TOL \Longrightarrow$ exit. $\underline{d}_n = \underline{d}^k_{n-1}$ Else : Carry out Newton-Raphson (N-R) Iterations until $\underline{R}\left(\underline{d}^k_{n-1}\right) \leq TOL \Longrightarrow$ exit. $\underline{d}_n = \underline{d}^k_{n-1} + \delta\underline{d}^k_{n-1}$
   (d) Determine $\vec{\sigma}$ for each element. Rotate $\vec{\sigma}$ along fiber direction.
   (e) Check for crack initiation in each element using failure criterion. If the criterion is not satisfied within a certain percentage (1%), reduce the increment size by a factor, go back to Step 1, and perform Steps a-e. Else, if the transition criterion is satisfied within a certain percentage (1%) $\Longrightarrow$ Separate the element along/perpendicular to fiber direction at the centroid of the element. Determine the modified element stiffness and force vector, and continue.
   (f) With modified assembled stiffness $\underline{K}$ and force vector $\underline{f}$, carry out N-R iterations. Solve for $\underline{d}_n$.
   (g) Check if the cohesive sub-element has met the failure criterion:
   If $\frac{G_I}{G_{IC}} + \frac{G_{II}}{G_{IIC}} \geq 1$: Element has broken completely
   Else, Element on the softening curve of the cohesive law
   (h) Store all information of softening elements, and continue to next increment(Step 1)

Figure 5. Algorithm for the CDFE method

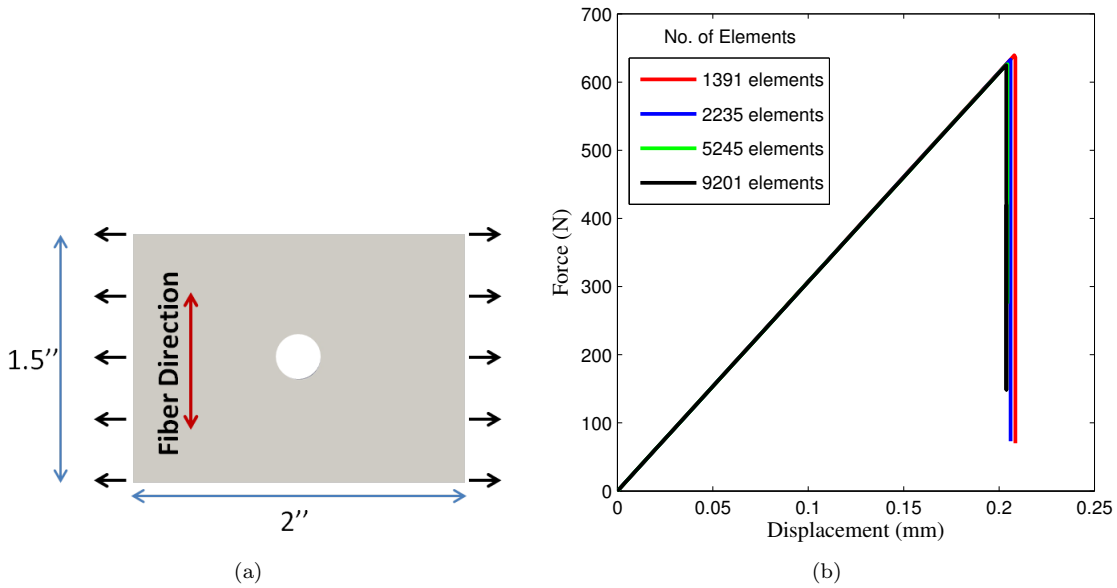

(a) (b)

Figure 6. (a) Schematic of a 90 degree lamina with a hole subjected to tension (b) Load - load-point extension plot of 90 degree plate with a hole

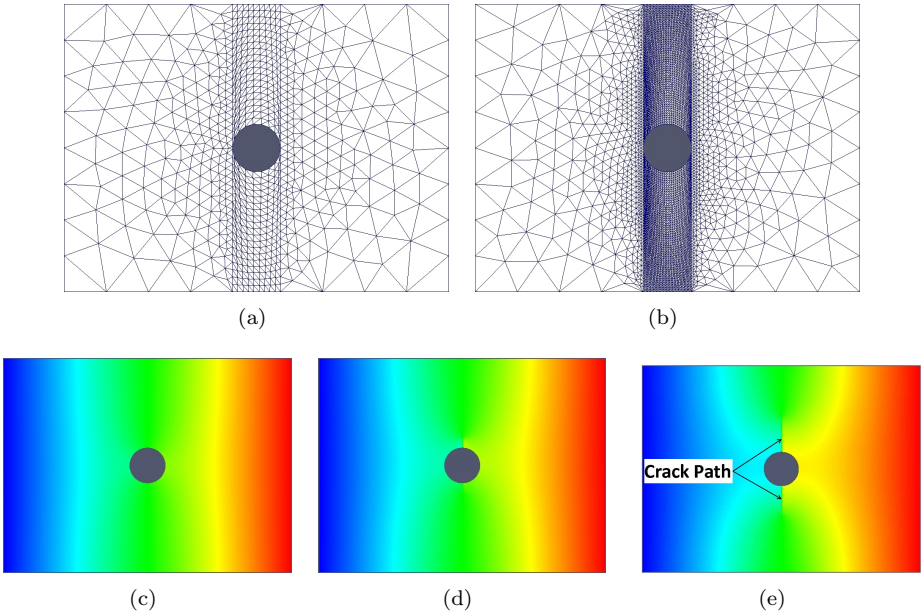

(a) (b)

(c) (d) (e)

Figure 7. Mesh refinement along the expected crack path (a) Coarse and (b) Fine. Displacement field from the simulation of a 90 degree lamina with a hole in tension at different loading stages; (c) Initial region, (d) Peak load and (e) Post-peak region

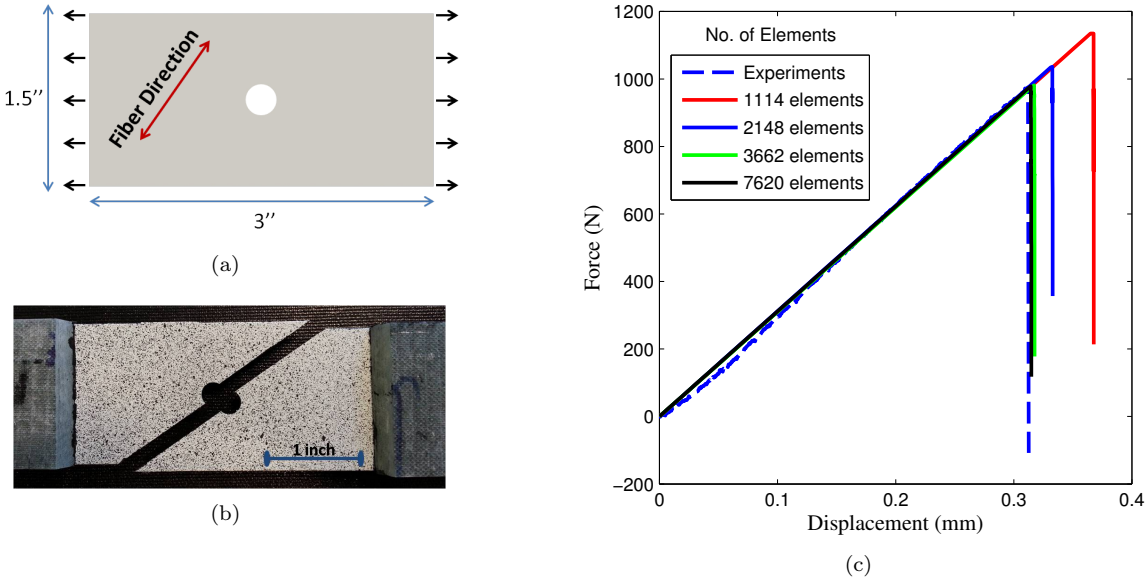

Figure 8. (a) Schematic of a 45 degree lamina with a hole subjected to tension (b) Failed specimen of a 45 degree lamina with a hole subjected to tension (c) Load - load-point extension plot of 45 degree plate with a hole

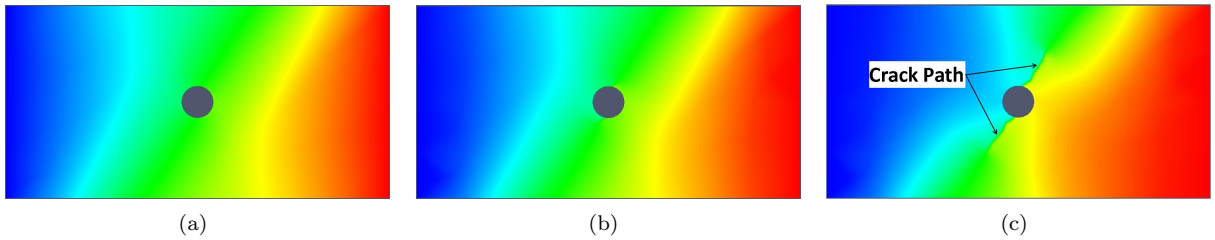

Figure 9. Displacement field from the simulation of a 45 degree lamina with a hole in tension at different loading stages; (a) Initial region, (b) Peak load and (c) Post-peak region

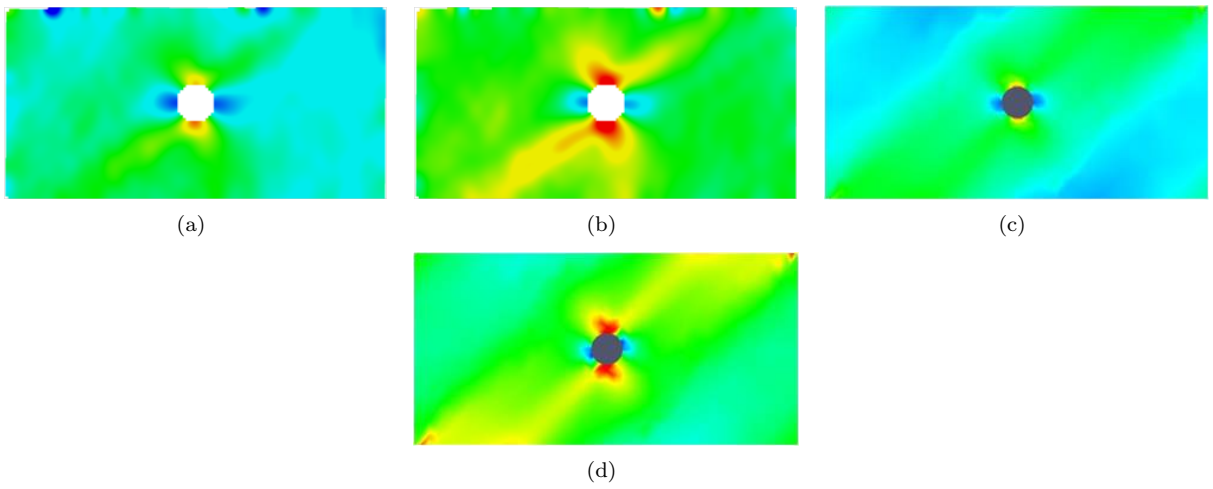

Figure 10. Axial strain field from DIC analysis of a 45 degree lamina with a hole in tension at different loading stages; (a) Initial region and (b) Peak load, and corresponding CDFE analysis in (c) and (d)

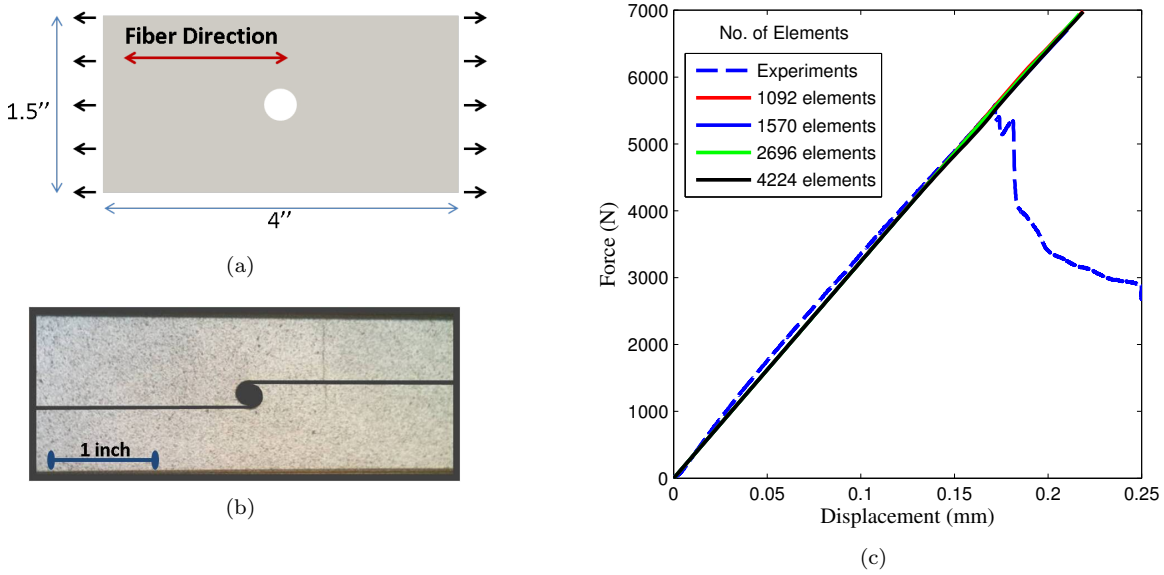

Figure 11. (a) Schematic of a 0 degree lamina with a hole subjected to tension (b) Failed specimen of a 0 degree lamina with a hole subjected to tension (c) Load - load-point extension plot of 0 degree plate with a hole

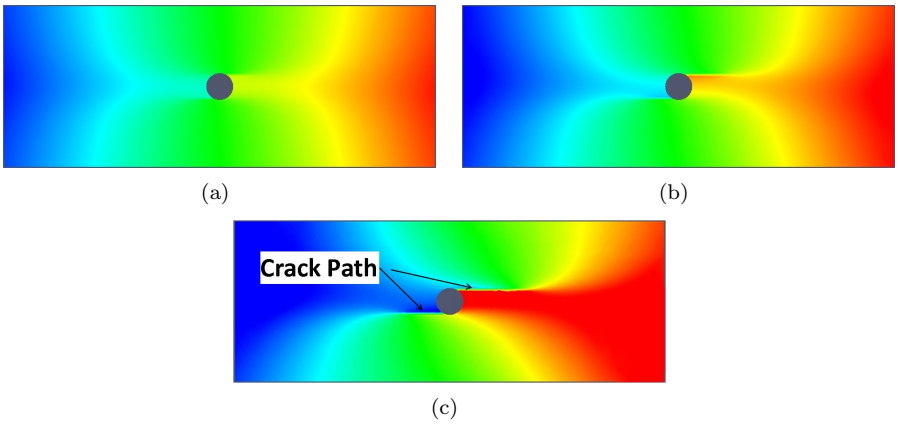

Figure 12. Displacement field from the simulation of a 0 degree lamina with a hole in tension at different loading stages; (a) Initial region, (b) Peak load and (c) Post-peak region

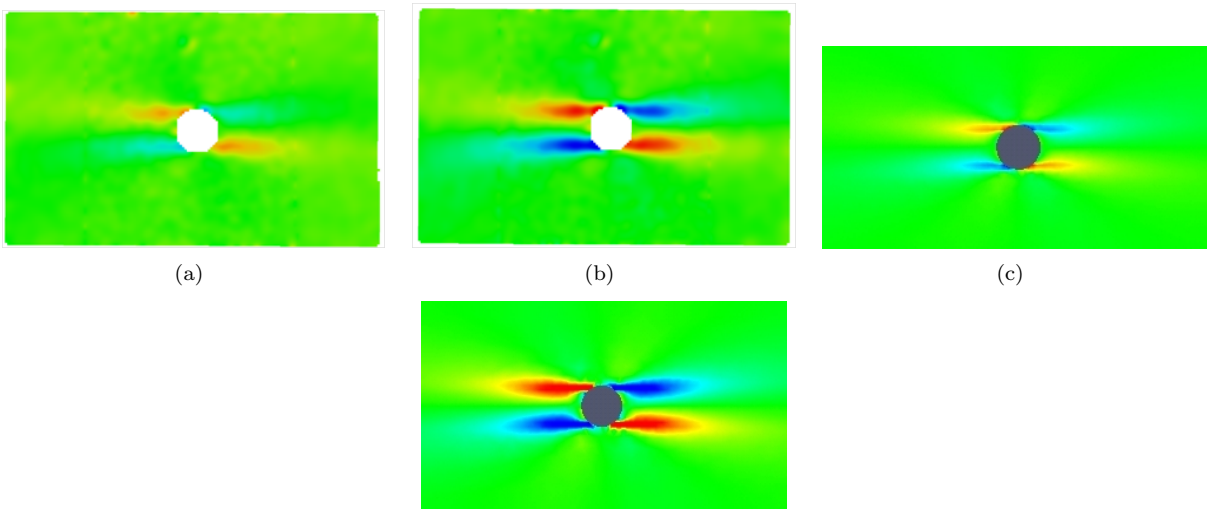

(a) (b) (c)

(d)

Figure 13. Shear strain field from DIC analysis of a 0 degree lamina with a hole in tension at different loading stages; (a) Initial region and (b) Peak load, and corresponding CDFE analysis in (c) and (d)